Experiment Shown in Fig. 1 is the layout of edge diagnostics and gas injectors. Two operating modes were used: a 3-4 MW NBI-heated L-mode, and a 4 MW NBI-heated H-mode with small and type I ELMs, with the L-H threshold at about 2.5 MW. The lower single null (LSN) divertor configuration with elongation $\kappa \leq 1.9$, triangularity $\delta \simeq 0.4$, and δr_{sep} of 1.0-1.5 cm was used. The plasmas had the following parameters: $B_t = 0.45$ T, $I_p = 0.7$ MA, $T_e(0) \simeq (0.8 - 1.0)$ keV, $\bar{n}_e \simeq (3-5) \times 10^{19}$ m^{-3} ($n_G \simeq 6 \times 10^{19}$ m^{-3}), $Z_{eff}(0) \leq 1.2 - 1.4$, $\tau_E \simeq 40$ ms. Deuterium was injected in an NBI-heated plasmas from the midplane high field side (HFS), midplane low field side (LFS) , and private flux region (PFR) gas injectors. Neon was injected from a midplane LFS injector in a separate experiment. Injections from the PFR resulted in a large increase in divertor neutral pressure from about 0.1 mTorr to 2 mTorr. The midplane pressure increase was from 0.05-0.10 mTorr to 0.1-0.15 mTorr. The neutral compression ratio measured in NSTX is typically 5 -10, thought to be a result of high wall structure conductances and a reduced plasma plugging effect.

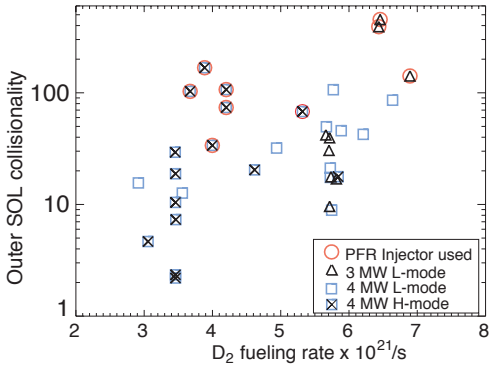

Figure 2: Outer SOL collisionality as a function of fueling rate and injector location

Results and discussion A compromise between the amount of injected gas needed to increase SOL collisionality to induce the outer leg detachment, and plasma operational limit was found by using the HFS and the PFR injectors together. The HFS and PFR injectors were used in an H-mode fueling rate scan, which produced clear signs of the outer strike point detachment. The HFS gas fueling is typically used for improved operational stability and H-mode access in NSTX [3], while adding an LFS injection would keep the plasma in an L-mode with the input power otherwise exceeding the H-mode power threshold. The gas injection rates were varied between 3 and 7 $\times 10^{21}$ s^{-1} in L-mode plasmas, and 3 and 4.5 $\times 10^{21}$ s^{-1} in H-mode plasmas, before inducing an H-L transition, confinement degradation or plasma termination due to MHD modes. At a HFS+LFS+PFR rate of 7×10^{21} s^{-1} the outer strike point was close to detachment, however at this fueling rate large MHD islands or a locked mode quickly degrade plasma confinement. The outer SOL collisionality, calculated from the Thomson scattering measurements, is proportional to the D_2 rate, with the largest $\nu^* > 60 - 80$ obtained with the PFR injector because of its higher fueling efficiency, and most of the LFS and HFS-fueled L-mode and H-mode points in the range $5 - 50$ (Fig. 2). This is consistent with the notion that the outer SOL in NSTX is in the sheath-limited and high-recycling regime with a weak parallel temperature gradient $dT_e/dx_{||}$ [6], with the typical upstream SOL temperature values in the range 10-60 eV. Shown in Fig. 3 (a) is the measured

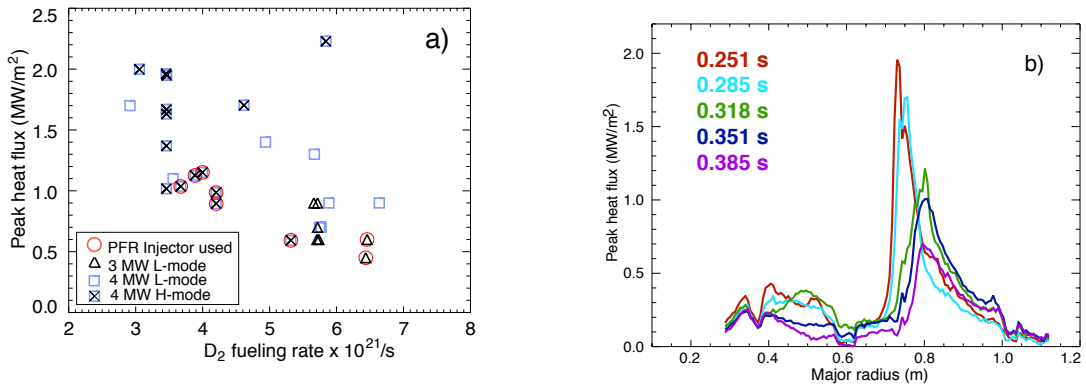

Figure 3: (a) Divertor outer heat flux as a function of fueling rate, (b) Divertor heat flux profile evolution as D_2 is injected at $t = 0.275$ s

divertor peak heat flux as a function of fueling rate. The inner divertor heat flux is practically unaffected by gas input as the inner divertor leg is detached. The outer divertor peak heat flux is reduced by a factor of 4 to about 0.5 MW/m^{-2} at the highest LFS+HFS fueling rate when the plasma is close to the operational limits. Similar reduction in heat flux is obtained with a much lower HFS+PFR fueling rate, without causing an H-L transition. Shown in Fig. 3 (b) are the divertor heat flux profiles obtained with an interim calibration from IRTV in the 4 MW H-mode plasma fueled from the HFS and PFR injectors. During the PFR-fueled phase the peak heat flux decreases and moves outward by up to 5 cm, possibly an indication of a partial detachment of the outer strike point [8]. The PFR-fueled phases were accompanied by a three-fold increase in core radiated power. The divertor radiated power is not fully accounted because of the poor bolometric coverage of the outer divertor (Fig. 1). Based on the total brightness, which weakly increases with gas fueling rate or input power, the divertor radiated power is estimated to be 10 % - 15 % of the total input power. If the fast ion losses are assumed to account for about 10-20 % of input power, as calculated by TRANSP, the power balance in the detached H-mode plasmas accounts for about 50-60 % of the input power, not far from the previously reported results [9].

The detachment of the outer divertor leg during PFR fueling is accompanied by the onset of volume recombination, as follows from the D_γ/D_α ratio measured by divertor cameras using an interim photometric calibration. The main recombination mechanisms in the cold high density plasmas are the radiative, 3-body and molecular assisted recombination. The recombination-populated high-n upper levels of atomic deuterium undergo spontaneous transitions yielding the characteristic Balmer series spectra otherwise unattainable through the electron excitation populating mechanism. Thus the D_γ/D_α ratio is used as a sensitive indicator of volume recombination in the divertor. The D_γ/D_α ratio is about 0.010-0.015 due to electron excitation, and 0.1 - 0.2 due to recombination for a range of T_e, n_e values typical for the divertor [10]. In Fig. 4(a). the D_γ/D_α ratio is plotted as a function of the quantity inverse to the SOL power per particle, n_{sep}/P_{SOL}. This quantity is indicative of conditions favoring the detachment in the operational P_{in}, n_e space. As the fueling rate is increased, n_{sep}/P_{SOL} also increased and the outer leg peak D_γ/D_α ratio approached the detached inner leg values 0.020-0.025. The ratios for the PFR fueling phase are among the highest, indicating the utility of the PFR injection for the outer divertor detachment. Plasma conditions in the detached inner divertor can be inferred from the Balmer series spectra. Example of a Balmer series spectra recorded by a spectrometer along the lines of sight labeled HID, VID in Fig. 1 is shown in Fig. 4 (b). The upper high-n level populations are in Saha-Boltzman equilibrium, and T_e can be estimated from their measured intensity ratios. Measured line profiles from photometrically calibrated spectra are numerically fitted with Voigt function profiles and their

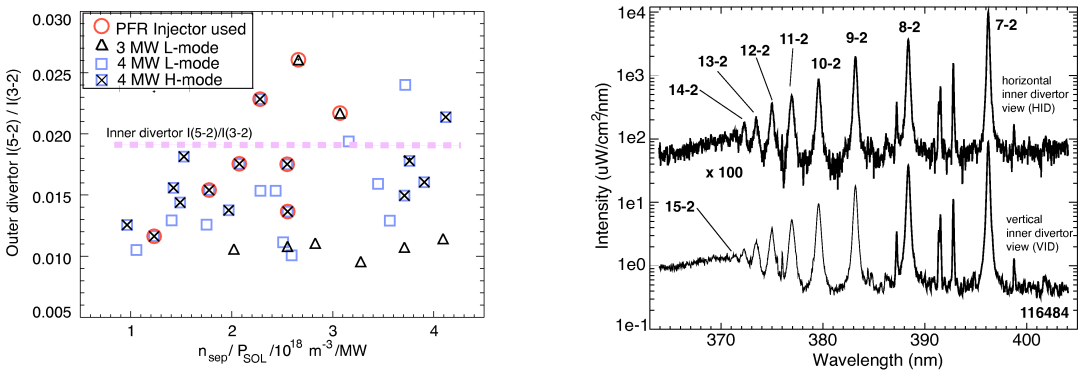

Figure 4: (a) Divertor D_γ/D_α ratio as a function of inverse upstream power per particle, (b) Balmer series spectra recorded from the detached inner divertor.

intensities are used to infer level populations using atomic data from [11]. Temperature in the range $T_e \simeq 0.4-1.0$ eV is inferred for the detached inner divertor leg using the $n = (11...7)-2$ transitions. Based on the highest observed level of the Balmer series $n = 15$ an approximate density $n_e < 10^{21}$ m^{-3} is inferred from the Inglis-Teller formula [12] for the inner divertor region. The analysis of the Stark broadening of the line corresponding to the $n = 8-2$ transition using the calculations from [13] indicated the density of $n_e < 2-7 \times 10^{20}$ m^{-3}. The conditions of the inner divertor leg are not only favorable for the onset of volume recombination but also for the formation of the radiative condensation instability [14] as carbon radiative cooling rate peaks in the range 5-10 eV. Bright radiation belts localized poloidally around the center stack and oscillating between inner divertor, X-point and inner midplane are observed by cameras in NSTX. The properties of these radiation belts and their role as sources and sinks for particles and heat are to be investigated.

In contrast to the D_2 experiments, neon injections did not result in the outer divertor detachment. Neon injection rate was scanned between 3 and 15 $\times 10^{19}$ s^{-1}. A 4 MW NBI-heated H-mode plasmas with the core P_{rad} fraction exceeding 30 % of the input power was obtained. The core radiated power profiles remained hollow, with a significant P_{rad} increase at the edge. Core Z_{eff} was $1.7-2.2$. Neon injection resulted in the four-fold reduction of the peak heat flux at the outer target, and slight broadening of the q_{out} profile, while the inner divertor peak heat flux decreased by 20 %. The divertor radiated power increase was a modest 10-20 %. However, the D_γ/D_α ratio in the outer divertor did not increase. While an additional power exhaust channel was established, the radiated power fraction was not sufficient to produce a detachment. Neon radiative cooling curve peaks at 80 eV which is apparently too high for NSTX SOL conditions to form a radiative divertor.

In summary, dedicated divertor detachment experiments have been conducted in NSTX using D_2 and neon injections into 3-4 MW NBI heated L- and H-mode plasmas. While the inner divertor detaches naturally at $\bar{n}_e \simeq 2-3 \times 10^{19}$ m^{-3} and input power $P_{in} \simeq 1$ MW, the detachment of the outer divertor only occurs at high divertor neutral densities and edge n_e obtained by direct D_2 injections into the PFR. The detachment is evidenced by a four-fold reduction of the peak heat flux and spectroscopic signatures of volume recombination. Future work will focus on detailed characterization of detached divertor conditions and further development of the heat flux mitigation scenarios with D_2 and low Z impurity gases.

Acknowledgments We thank D. Mastrovito, R. Gernhardt and P. Roney for computer and technical support, and T. Stevenson and D. Gates for operating NSTX. This research is supported by the U.S. Department of Energy under contracts No. W-7405-Eng-48, DE-AC02-76CH03073, DE-AC05-00OR22725, and W-7405-ENG-36.

[1] P. C. Stangeby, *The plasma boundary of Magnetic Fusion Devices* (IoP, Bristol, 2000).
[2] R. Stambaugh, et al, Nuclear Fusion **39**, 2391 (1999).
[3] R. Maingi, et al, Nuc. Fusion **43**, 969 (2003).
[4] R. Maingi, et al, Nucl. Fusion **45**, 264 (2005).
[5] V. A. Soukhanovskii, et al, in *Proc. 30th EPS Conf. on Control. Fus. and Plasma Phys.* (ECA, St. Petersburg, Russia, 2003), Vol. 27A, pp. P–3.179.
[6] V. A. Soukhanovskii, et al, J. Nuc. Mater. **337-339**, 475 (2005).
[7] D. Post, et al, J. Nuc. Mater. **220-222**, 1014 (1995).
[8] T.W. Petrie, et al, Nuc. Fusion **37**, 321 (1997).
[9] S. F. Paul, et al, J. Nuc. Mater. **337-339**, 251 (2005).
[10] G. M. McCracken, et. al., Nuc. Fusion **38**, 619 (1998).
[11] L. Johnson and E. Hinnov, J. Quant. Spectrosc. Radiat. Transf. (UK) **13**, 333 (1973).
[12] D. Inglis and E. Teller, Astrophysical Journal **90**, 439 (1939).
[13] R. Bengston, et al, Phys. Rev. A **1**, 532 (1970).
[14] B. Lipschultz, et al, Nuc. Fusion **24**, 977 (1984).